Binding of Plasminogen and Tissue Plasminogen Activator to Plasmin-Modulated Factor X and Factor Xa†

J. E. Grundy,‡ N. Lavigne,‡ T. Hirama,§ C. R. MacKenzie,§ and E. L. G. Pryzdial*,‡,||

R&D Department, Canadian Blood Services, 1800 Alta Vista Drive, Ottawa, Ontario, Canada K1G 4J5

Received September 19, 2000; Revised Manuscript Received March 28, 2001

ABSTRACT: Previous work in our laboratory has suggested that the fibrinolytic enzyme plasmin (Pn) inactivates coagulation factors X (FX) and Xa (FXa) in the presence of Ca^{2+} and anionic phospholipid (aPL), producing fragments which bind plasminogen (Pg) and accelerate tissue plasminogen activator (t-PA). Our goals here were to determine if the Pn-mediated fragments of FX or FXa remain associated, whether they directly bind t-PA, and to quantify their interaction with Pg. Binding to aPL, benzamidine-Sepharose, or the active-site inhibitor dansyl-Glu-Gly-Arg-chloromethyl ketone demonstrated that Pn cleavage yielded noncovalent heterodimers of a fragment containing the aPL-binding domain ($FX\gamma_{47}$ or $FXa\gamma_{33}$) and a 13-kDa fragment ($FX\gamma_{13}$ or $FXa\gamma_{13}$). Both ligand blotting and surface plasmon resonance (SPR) showed that Pn-cleaved FX and FXa bound t-PA directly when Pn-treatment was effected in the presence of aPL and Ca^{2+}. Using SPR, apparent K_d values of 1−3 μM and 0.3−0.4 μM were measured directly and by competition for the $FX\gamma_{47/13}$−Pg and $FXa\gamma_{33/13}$−Pg interactions, respectively. For the first time, Pg-binding to a receptor was shown to be Ca^{2+} enhanced, although primarily mediated by C-terminal lysine residues. Mathematical modeling of kinetic data suggesting two Pg per $FX\gamma_{47/13}$ or $FXa\gamma_{33/13}$ was consistent with our conclusion that each subunit of $FX\gamma_{47/13}$ or $FXa\gamma_{33/13}$ contains a C-terminal lysine. Earlier X-ray structures show that these Lys residues are distal from each other and the membrane, supporting the model where each interacts with a separate Pg. t-PA acceleration by $FX\gamma_{47/13}$ or $FXa\gamma_{33/13}$ may therefore involve simultaneous presentation of two substrate molecules.

Factor Xa (FXa)[1] is a serine protease which participates along with the nonenzymatic cofactor, factor Va, to produce thrombin, the principal effector of blood coagulation. Both FXa and its zymogen, factor X (FX) are composed of a light chain (amino acids 1−139)[2] linked by a single disulfide bond to a heavy chain (amino acids 143−448 for FX; cleaved to 195−448 for FXa) (*2*). The light subunit of FX and FXa mediates Ca^{2+}-dependent binding to anionic phospholipid (aPL) through a γ-carboxyglutamic acid (Gla) domain (*3*, *4*), while the heavy subunit contains a trypsin-like serine protease catalytic domain (*2*). The focus of the current manuscript is a mechanism emerging from our previous work suggesting that the fibrinolytic enzyme Pn modulates the function of aPL-bound FX and FXa from coagulation components to fibrinolysis accelerators. At the same time, Pn cleavage of FX and FXa destroys amidolytic activity and participation in coagulation (*5*−*7*).

FXa and FX fragmentation by Pn is summarized in Figure 1. FXaα bound to aPL is rapidly converted by Pn to FXaβ by a cleavage predicted to be after Lys^{435}. Subsequent Pn cleavage after Lys^{330} generates a 33-kDa ($FXa\gamma_{33}$) and a 13-kDa fragment ($FXa\gamma_{13}$), collectively termed $FXa\gamma_{33/13}$. These products are similar to those of FXa autoproteolysis (Figure 1) (*6*, *8*−*11*); however, on a molar basis, Pn produces these species 3 orders of magnitude faster (*6*). Cleavage in the autolysis loop correlates to loss of FXa enzymatic activity (*6*, *11*). FX bound to aPL is cleaved after Lys^{435} and Lys^{330} to yield FXβ, a 47-kDa fragment ($FX\gamma_{47}$) and a 13-kDa fragment ($FX\gamma_{13}$), respectively (collectively termed $FX\gamma_{47/13}$). This is followed by an additional heavy-chain cleavage after Arg^{295} (not seen under these conditions for FXa), to generate a 28-kDa fragment ($FX\delta_{28}$) (*7*). In this study we considered the effects of the major products of Pn proteolysis under aPL-binding conditions, namely $FX\gamma_{47/13}$ and $FXa\gamma_{33/13}$, which are different solely in the activation fragment. When proteolysis occurred in the absence of either aPL or Ca^{2+},

† Supported by an Industrial Research Fellowship from the Natural Sciences and Engineering Research Council of Canada (J.G.), a Career Development Fellowship Award from Canadian Blood Services (J.G.), by a Heart and Stroke Foundation of Canada Operating Grant (E.P.) and the Canadian Blood Services R&D Fund (E.P.).

* To whom correspondence should be addressed. Phone: (613) 739-2462. Fax: (613) 739-2201. E-mail: ed.pryzdial@bloodservices.ca.

‡ Canadian Blood Services.

§ Institute of Biological Sciences, National Research Council of Canada, Ottawa, Ontario, Canada K1A 0R6.

|| Department of Biochemistry, Microbiology and Immunology, University of Ottawa, Ottawa, Ontario, Canada K1H 8M5.

[1] Abbreviations: t-PA, tissue-type plasminogen activator; Pg, plasminogen; Pn, plasmin; FX, factor X; FXa, activated factor X; $FX\gamma_{47/13}$, Pn-cleaved FX generated in the presence of anionic phospholipid and calcium; $FXa\gamma_{33/13}$, Pn-cleaved FXa generated in the presence of anionic phospholipid and calcium, aPL, anionic (procoagulant) phospholipid; SDS−PAGE, sodium dodecyl sulfate polyacrylamide gel electrophoresis; KIU, kallikrein inhibitory units; GEMSA, 2-guanidinoethyl mercaptosuccinic acid; HEPES, *N*-[2-hydroxyethyl]-piperazine-*N*′-[2-ethanesulfonic acid]; HBS, 20 mM HEPES, 150 mM NaCl, pH 7.4; SPR, surface plasmon resonance; DEGR-ck, dansyl-Glu-Gly-Arg-chloromethyl ketone; EDTA, ethylenediamine tetraacetic acid; RU, resonance units; BIA, biospecific interaction analysis; ϵ-ACA, 6-aminocaproic acid; PCPS, 75% phosphatidylcholine, 25% phosphatidylserine; Gla, γ-carboxyglutamic acid.

[2] Numbering based on the amino acid sequence predicted from FX cDNA (*1*).

10.1021/bi002209v CCC: $20.00 © 2001 American Chemical Society
Published on Web 05/03/2001

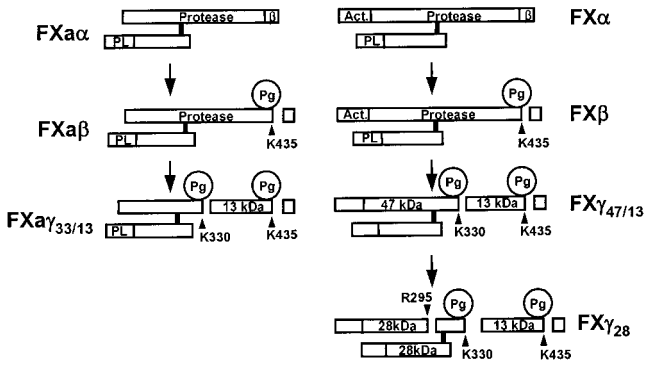

FIGURE 1: Fragmentation of FXa and FX by Pn. Pn cleavage of FXa or FX under aPL-binding conditions occurs only in the heavy chain and yields products with C-terminal lysine residues. The peptides generated as a result of cleavage have been shown to bind Pg, in agreement with previous results showing Pg localization to phospholipid by Pn-cleaved FXa and t-PA acceleration by Pn-cleaved FX or FXa. The largest fragment contains the aPL-binding Gla-domain. Adapted from Pryzdial and Kessler (*6*) and Pryzdial et al. (*7*). Act., activation peptide which is cleaved in FX to produce FXa. PL, aPL-binding Gla domain. Protease, catalytic domain of FX or FXa.

products were formed which were structurally and functionally different, with cleavages after Arg^{429} and Lys^{43} destroying coagulation activity presumably by disrupting aPL-binding (*6*).

To explain the participation of FXa$\gamma_{33/13}$ and FX$\gamma_{47/13}$ in the fibrinolysis pathway, each has predicted newly exposed C-terminal lysine residues, which are well-known essential characteristics of Pg receptors (*5*, *12*−*20*). The products of Pn cleavage of FXa and FX were accordingly shown to act as Pg receptors in ligand blots (*6*, *7*) and to accelerate tissue Pg activator (t-PA), resulting in enhanced Pn generation (*5*−*7*). To estimate the affinity of Pn-cleaved FXa binding to Pg, equilibrium binding studies were conducted ($K_d = 0.29$ μM) (*5*). Although informative, these early experiments utilized uncharacterized FXa cleavage products. Additionally, t-PA binding to Pn-cleaved FXa or FX has only been inferred from functional assays and no direct evidence for binding has been obtained. In the current work we have characterized the noncovalent subunit composition of aPL-bound FX$\gamma_{47/13}$ and FXa$\gamma_{33/13}$, conducted direct binding studies to demonstrate the interaction of FX$\gamma_{47/13}$ and FXa$\gamma_{33/13}$ with t-PA, and quantified the interaction of well-characterized FX$\gamma_{47/13}$ or FXa$\gamma_{33/13}$ with Pg.

EXPERIMENTAL PROCEDURES

Chemicals and Reagents. HEPES, EDTA, bovine serum albumin (BSA), ϵ-aminocaproic acid (ϵ-ACA), phosphatidylcholine (PC), and phosphatidylserine (PS) were purchased from Sigma. t-PA stimulator (CNBr-cleaved fibrinogen fragment FC-2), chromogenic substrates S-2238 (D-Phe-Pip-Arg-*para*-nitroanilide), S-2251 (D-Val-Leu-Lys-*para*-nitroanilide), and S-2765 (*N*-α-Cbo-D-Arg-Gly-Arg-*p*-nitroanilide) were purchased from Chromogenix. The bicinchoninic acid (BCA) protein assay kit, Iodogen and Exocellulose 5 columns were purchased from Pierce. Aprotinin, dansyl-Glu-Gly-Arg-chloromethyl ketone (DEGR-ck), carboxypeptidase B and 2-guanidinoethyl mercaptosuccinic acid (GEMSA) were purchased from Calbiochem. Human FX, FXa, Pg (Lys-plasminogen) and Pn were purchased from Haematologic Technologies, Inc. Recombinant single-chain t-PA was purchased from Genentech. ^{125}I, benzamidine-Sepharose 6B and ECL chemiluminescent substrate kit were purchased from Amersham Pharmacia Biotech. t-PA was radiolabeled with ^{125}I using Iodogen in accordance with the manufacturer's recommendations (Pierce). Unincorporated ^{125}I was removed by chomatography with Exocellulose 5. Activity of unlabeled and radiolabeled t-PA was assessed by its ability to catalyze Pg activation, by detection of S-2251 hydrolysis in the presence and absence of CNBr-cleaved fibrinogen. In all cases, specific activity of radioiodinated protein was similar to unlabeled protein. [^{125}I]t-PA was labeled to 165 000 cpm/μg protein.

Small unilamellar vesicles (SUV; average diameter: 50 nm) containing 100% PC or a 75:25 mixture of phosphatidylcholine/phosphatidylserine (PCPS) were prepared as described (*21*). Large vesicles (LV; average diameter 300−600 nm) were made as follows: 1−4 mg of phosphatidylcholine (PC) or PCPS was suspended in 1 mL of methanol in glass tubes and dried to a thin film under a stream of nitrogen at 4 °C, followed by incubation in a desiccator under vacuum overnight, at 4 °C. The thin lipid layer was resuspended in 0.5−1.0 mL of 20 mM HEPES, 300 mM sucrose, pH 7.4, vortexed for 1 min, then transferred to a plastic vial. The suspension was frozen and thawed 10 times, then extruded through two 1 μm filters using a Liposofast Basic (Avestin, Ottawa, ON) and collected into an eppendorf tube. LV were mixed 1:1 with HBS and pelleted by centrifugation at 13000*g* for 2−5 min at room temperature. Vesicles were resuspended in HBS, kept at 4 °C, and used within two weeks. SUVs and LVs were sized by laser light scattering; vesicle size was not different for fresh or month-old vesicles. Phospholipid concentrations were determined using an assay for total phosphorus (*22*). FX$\gamma_{47/13}$ and FXa$\gamma_{33/13}$ generated in the presence of LV were identical to those obtained with SUV (data not shown).

Plasmin Cleavage of FX and FXa. All experimental steps were conducted at room temperature, except where indicated. FX (9 μM) or FXa (5 μM) was treated with 0.1 μM Pn in HBS in the presence of 300 μM SUV made with PC or PCPS, with either 2 mM Ca^{2+} or 5 mM EDTA, as described previously (*7*). GEMSA (50 nM) was added either during or immediately following Pn cleavage, to inhibit any possible carboxypeptidase B-like activity. Aprotinin was added to a final concentration of 50 kallikrein inhibitory units (KIU)/mL to stop Pn activity. All reactions yielded residual amounts of FXβ and FXaβ which were estimated at less than 10% of total protein, by Coomassie blue staining. FX$\gamma_{47/13}$ and FXa$\gamma_{33/13}$ were confirmed to accelerate t-PA, and Pn-cleaved FX and FXa fragments generated in the absence of Ca^{2+} and/or aPL were confirmed not to accelerate t-PA, as described previously (*5*−*7*).

Isolation of FX$\gamma_{47/13}$ or FXa$\gamma_{33/13}$ from Phospholipid Using LV. Vesicles larger than 100 nm in diameter are multilamellar, and thus present a smaller surface-to-phospholipid ratio for FXa binding than SUV. To account for this difference, 900 μM PCPS LV were used instead of 300 μM and experimentally determined to give the same cleavage patterns. FX (9 μM) or FXa (5 μM) was treated with 0.1 μM Pn in 20 mM HEPES, 150 mM NaCl, pH 7.2 in the presence of 900 μM large PCPS or PC vesicles. In the case of PCPS vesicles, either 2 mM Ca^{2+} or 5 mM EDTA was

included in the reaction. For PC vesicles, only Ca^{2+} was included in the reaction. Following incubation, vesicles were collected by centrifugation at 13000*g* for 10 min at room temperature. The pellet was resuspended in HBS containing 5 mM EDTA, 50 KIU/mL aprotinin, and 50 nM GEMSA, and was incubated for 20 min at room temperature. Vesicles were again collected by centrifugation and the supernatant was removed and recalcified to a final concentration of 10 mM.

Reassociation of FX$\gamma_{47/13}$ and FXa$\gamma_{33/13}$ to Phospholipid. To detect reassociation of FX$\gamma_{47/13}$ or FXa$\gamma_{33/13}$ with phospholipid, FX or FXa was cleaved with plasmin on 900 μM LV as described above, and released by treatment with 5 mM EDTA. After centrifugation of LV, phospholipid-depleted supernatants were collected and recalcified to 10 mM. A fresh aliquot of LV was added to the supernatant, to a final concentration of 900 μM. After a 5 min incubation, the vesicles were collected by centrifugation. FX$\gamma_{47/13}$ and FXa$\gamma_{33/13}$ separated on nonreducing SDS−PAGE were detected by Coomassie or silver staining. Residual phospholipid in the final products was measured to be 0.09 μM. Assuming the residual phospholipid to be in the form of SUV, 24 nM of the residual phospholipid was PS, with 11 nM of the PS presumed exposed on the surface of vesicles, assuming 59% of the lipids on the outer surface and an equal distribution of lipids in vesicles (*21*). As the aPL-binding domain of FX$\gamma_{47/13}$ or FXa$\gamma_{33/13}$ is unchanged from the native protein and accounts for all aPL-binding character of FX or FXa, the cleaved species are proposed to have the same affinity for aPL as their uncleaved precursors. Based on a predicted stoichiometry of 11.5:1 of PS:FXa (*23*), less than 0.02% of FXa$\gamma_{33/13}$ would be bound to phospholipid in aPL-depleted preparations. This small amount was assumed to have a negligible effect on binding of FX$\gamma_{47/13}$ or FXa$\gamma_{33/13}$ to Pg observed by surface plasmon resonance.

Incorporation of Protease Active-Site Inhibitors into FXa$\gamma_{33/13}$. Benzamidine-Sepharose 6B was mixed with FXa$\gamma_{33/13}$ created in the presence of SUV. After 20 min, the benzamidine-Sepharose was pelleted by centrifugation, washed with HBS and transferred to SDS-buffer for nonreducing SDS−PAGE. Incorporation of DEGR-ck into FXa$\gamma_{33/13}$ bound to SUV was accomplished as previously described for FXa (*24*). The products were separated on nonreducing SDS−PAGE and visualized on a UV light box.

Ligand Blots. FX and FXa were Pn-cleaved as described previously. Digests were sampled over time directly into SDS-buffer for electrophoresis. Ligand blotting was performed essentially as described previously (*6*, *7*). Briefly, PVDF blots of cleaved FX or FXa were exposed to 0.1 μM [^{125}I]t-PA in 20 mM Tris, 150 mM NaCl, pH 7.4 (TBS), containing 10 mg/mL BSA. Band patterns obtained with autoradiography were compared to the electrophoretic patterns made visible by staining gels of the same samples with Coomassie Brilliant Blue G-250 or silver nitrate.

Surface Plasmon Resonance. FX or FXa were cleaved with Pn as described above. The interaction of Pn-cleaved FX or FXa with immobilized t-PA or Pg was observed using a BIAcore 1000 or 3000 biosensor system (*25*) (Biacore, Piscataway, NJ). Between 2000 and 13000 resonance units (RU) of Pg (0.02−0.16 pmol/mm^2) or t-PA (0.03−0.22 pmol/mm^2) were immobilized on flow cells of research grade CM5 sensor chips (Biacore) by amine coupling at pH 4.5, 5 μL/min, as described previously (*26*). For proteins, 1 RU generally corresponds to an immobilized protein concentration of ~1 pg/mm^2. However other compounds, such as vesicles, also contribute to the RU. Preparations of Pn-cleaved FX and FXa produced in the presence of SUV and Ca^{2+} or EDTA were diluted in running buffer (HBS with 50 KIU aprotinin/mL, 50 nM GEMSA and 2 mM Ca^{2+}) and injected over the differently coated flow cells at 5 μL/min, to view association with Pg or t-PA. Binding was observed as an increase in resonance units (RU) over time. Dissociation was shown by a decrease in RU when the injection was terminated, and flow was switched to buffer. To determine specificity, preparations of FXa$\gamma_{33/13}$ or FX$\gamma_{47/13}$ cleaved in the presence of Ca^{2+} and aPL were injected over flow cells coated with irrelevant protein (monoclonal anti-*Salmonella* serogroup B lipopolysaccharide, BSA immobilized on a sensor chip) or uncoated dextran.

Although the interaction in the presence of phospholipid may be more representative of physiological events, measurement of the kinetics of the intrinsic interaction between FX$\gamma_{47/13}$ or FXa$\gamma_{33/13}$ and Pg required that the phospholipid be removed following Pn cleavage. To accomplish this, we used LV as described above to aPL-deplete FX$\gamma_{47/13}$ or FXa$\gamma_{33/13}$. BSA (0.1%), 50 KIU aprotinin, 50 nM GEMSA, and concentrations of Ca^{2+} as described in each experiment were included in the SPR running buffer for experiments using aPL-depleted FX$\gamma_{47/13}$ or FXa$\gamma_{33/13}$.

To kinetically derive the dissociation constant of FX$\gamma_{47/13}$ or FXa$\gamma_{33/13}$ fragment-binding to Pg, aPL-depleted FX$\gamma_{47/13}$ or FXa$\gamma_{33/13}$ were titrated onto 2000 RU of immobilized Pg, at 20 μL/min. The same solutions were tested on a surface of irrelevant protein, where no binding was observed. To determine the simplest mathematical model adequately representing the data, titrations were analyzed using nonlinear fitting of the primary SPR data using the BIAevaluation 2.0 software (BIAcore) to both a 1:1 and a 1:2 model of binding.

Univalent model:

$$A + B \underset{k_{-1}}{\overset{k_1}{\rightleftharpoons}} AB \qquad (1)$$

where A = concentration of unbound FX$\gamma_{47/13}$ or FXa$\gamma_{33/13}$, B = unbound Pg, AB = bimolecular complex (e.g., FXa$\gamma_{33/13}$−Pg), k_1 = rate of formation of AB, and k_{-1} = rate of dissociation of AB. In this model, the rate equation is as follows:

$$\frac{dAB}{dt} = (k_1 \times A \times B) - (k_{-1} \times AB) \qquad (2)$$

In addition to applying the above fit to the data, the BIAevaluation software takes into account changes which may occur due to a solution with a different refractive index from the running buffer being injected over the sensorchip (i.e., "bulk change" effects).

The next-simplest fit to which the data was applied was a model wherein one FX$\gamma_{47/13}$ or FXa$\gamma_{33/13}$ sequentially binds two Pg. Binding to the first Pg molecule and second Pg molecule is described by separate sets of rate constants.

Bivalent model:

$$A + 2B \underset{k_{-1}}{\overset{k_1}{\rightleftharpoons}} AB + B \underset{k_{-2}}{\overset{k_2}{\rightleftharpoons}} ABB \qquad (3)$$

where AB and ABB = bimolecular (i.e., FXa$\gamma_{33/13}$−Pg) and

trimolecular [i.e., FXa$\gamma_{33/13}$-$(Pg)_2$] complexes formed, respectively. Respective rates of association (k_1, k_2) and dissociation (k_{-1}, k_{-2}) for each step are shown. The rate equations describing formation of AB and ABB (*27*) are shown below:

$$\frac{dAB}{dt} = [(2 \times k_1) \times A \times B - k_{-1} \times AB) - (k_2 \times AB \times B - (2 \times k_{-2}) \times ABB] \quad (4)$$

$$\frac{dABB}{dt} = [k_2 \times AB \times B - (2 \times k_{-2}) \times ABB] \quad (5)$$

K_{d1} and K_{d2} of FX$\gamma_{47/13}$ or FXa$\gamma_{33/13}$ from Pg were calculated from k_{-1}/k_1 and k_{-2}/k_2, which were kinetically derived by fitting the data to the above model. Since k_2 represents the rate of formation of ABB from AB + B (eq 3) and AB is reported in RU, the value of k_2 is initially returned (RU^{-1} s^{-1}) by BIAevaluation software. This was converted to $M^{-1}sec^{-1}$ by multiplication of k_2 by the molecular weight of the ligand (Lys-Pg; 83 000 Da) and by a conversion factor of 100.

As a second estimate of K_d, and to determine if amine coupling affected the conformation of Pg bound to the flow cell, competition experiments were conducted to show that free Pg could inhibit FX$\gamma_{47/13}$ or FXa$\gamma_{33/13}$ bound to immobilized Pg on the flow cell. Here, the concentration of FX$\gamma_{47/13}$ or FXa$\gamma_{33/13}$ was held constant at 0.625 or 0.7 μM, respectively and solution-phase Pg was titrated. To account for any possible association of solution-phase Pg with Pg coupled to the BIAchip flow cell, mixtures were injected which included all components except FX$\gamma_{47/13}$ or FXa$\gamma_{33/13}$, but no binding was observed. The different concentrations of Pg in each injection resulted in a constant refractive index change (called a "bulk change") from the start to end of each injection, proportional to the concentration of free Pg in the injection but unrelated to any interaction of FXa$\gamma_{33/13}$ with Pg. At the end of each injection the bulk change disappeared within 5 s as the running buffer flow resumed, and the resonance units dropped to a value proportional only to the amount of bound FXa$\gamma_{33/13}$. This point (5 s after injection) was taken as maximal RU at the start of dissociation, and was plotted vs concentration of added Pg to obtain an inhibition curve and fit using Marquhart−Levenberg minimization to the following equation:

$$v = v_0 \times I_{50}/(I_{50} + [I]) \quad (6)$$

where v_0 = initial velocity, I_{50} = [I] at which $v = v_0/2$, and [I] = [added or solution Pg].

Calcium-Dependence and Binding Specificity. To determine whether binding of FX$\gamma_{47/13}$ or FXa$\gamma_{33/13}$ to immobilized Pg was calcium-dependent, aPL-depleted FX$\gamma_{47/13}$ or FXa$\gamma_{33/13}$ (not recalcified) was mixed with running buffer with various concentrations of Ca^{2+}. Equilibration and injection in running buffer containing 5 mM EDTA was also performed. Following a short period of incubation (10−20 min at room temperature), the same buffer used to equilibrate the FX$\gamma_{47/13}$ or FXa$\gamma_{33/13}$ was used to prime the BIAcore, and mixtures were injected at 5 μL/min for 6 min over 2000 RU of immobilized Pg. Available Ca^{2+} was estimated by subtraction of residual EDTA present in FXa$\gamma_{33/13}$ injections (0.375 mM). SPR data were fit to 1:1 and 1:2 binding models as described previously.

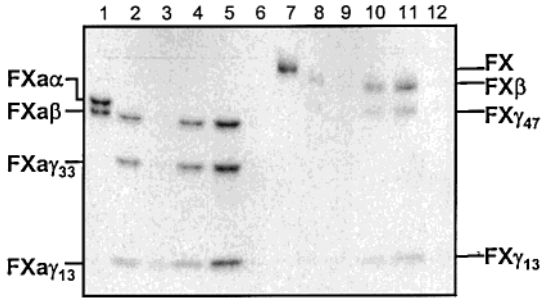

FIGURE 2: Association of Pn-cleaved FX and FXa fragments. Uncleaved FXa, lane 1. Following cleavage with 0.1 μM Pn in the presence of PCPS LV (900 μM) and Ca^{2+} (2 mM), vesicles were collected by centrifugation (lane 2) then were separated from phospholipid by incubation in 5 mM EDTA. The preparation was centrifuged to separate dissociated FXa fragments and phospholipid (pellet, lane 3; supernatant, lane 4). FXa fragments in supernatant were recalcified to a final concentration of 20 mM Ca^{2+}. PCPS LV (900 μM) were added and the mixture incubated for 10 min at room temperature, followed by centrifugation to collect the pellet (pellet, lane 5; supernatant, lane 6). FX (lane 7) was treated similarly to FXa (lanes 8−12).

To test whether the interaction of Pg with FX$\gamma_{47/13}$ or FXa$\gamma_{33/13}$ was mediated by C-terminal lysines, the C-terminal lysine analogue ϵ-ACA (5 mM) was mixed with FX$\gamma_{47/13}$ or FXa$\gamma_{33/13}$ prior to injection. Running buffer contained 2 mM Ca^{2+}. In other experiments, 48 units/mL carboxypeptidase B, which cleaves C-terminal lysine residues, was mixed with FX$\gamma_{47/13}$ or FXa$\gamma_{33/13}$, prior to injection.

RESULTS

Noncovalent Association of FX$\gamma_{47/13}$ or FXa$\gamma_{33/13}$ Fragments. Pn cleavage of FX or FXa in the presence of Ca^{2+} and aPL yields a 47- or 33-kDa fragment, respectively, which contain the entire aPL-binding light domain, and a 13-kDa fragment, from the C-terminal end of the heavy subunit (*6*, *7*). To determine whether the cleaved proteins were noncovalent heterodimers, FX$\gamma_{47/13}$ or FXa$\gamma_{33/13}$ were generated on PCPS-containing LV in the presence of Ca^{2+}. Upon centrifugation of the LV to collect bound protein, both 47- and 13-kDa fragments were observed for cleaved FX (FXγ_{47} and FXγ_{13}), and 33- and 13-kDa fragments were observed for FXa (FXaγ_{33} and FXaγ_{13}) in equal proportions, by Coomassie staining (Figure 2). Upon EDTA extraction, both components of FX$\gamma_{47/13}$ and FXa$\gamma_{33/13}$ dissociated quantitatively from aPL, due to the known Ca^{2+} dependence of FX and FXa binding to aPL. When fresh LV were mixed with the recalcified fragments, FX$\gamma_{47/13}$ or FXa$\gamma_{33/13}$ were observed to rebind to LV. The reassociation was dependent on the presence of aPL (PS) in the vesicles. Since only FXγ_{47} or FXaγ_{33} contains the aPL-binding Gla-domain, this result provided strong evidence that the 13-kDa fragment from Pn-cleaved FX or FXa remained noncovalently associated with the larger fragment.

Since aPL-affinity fractionation with LV showed that FXa$\gamma_{33/13}$ subunits did not dissociate from one another, the structure of the cleaved molecule was investigated further by incubation of FXa$\gamma_{33/13}$ with the specific active site probes DEGR-ck, which requires residues in both fragments of FXa$\gamma_{33/13}$ (Figure 3A) and benzamidine, which requires residues only in the 13 kDa fragment for binding (Figure 3B). Incorporation of the fluorescent active site modifier

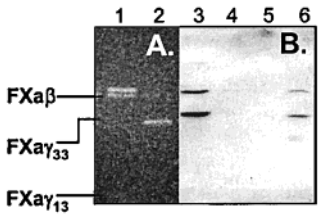

FIGURE 3: Incorporation of protease active site inhibitors into Pn-cleaved FXa. (A) FXa$\gamma_{33/13}$ was produced in the presence of PCPS SUV. Products were mixed with DEGR-ck and viewed using nonreduced SDS−PAGE (12% acrylamide) under UV light. Lane 1, untreated FXa; lane 2, FXa$\gamma_{33/13}$. (B) FXa$\gamma_{33/13}$ fragments were prepared on PCPS LV as described in Materials and Methods. Following cleavage, fragments were dissociated from PCPS LV by extraction with EDTA. Cleaved FXa was mixed with benzamidine-Sepharose 6B. Lane 3, Pn-derived FXa fragments after extraction from LV, supernatant, lane 4, pellet. FXa fragments in lane 3 were mixed with benzamidine-Sepharose 6B, lanes 5 and 6, supernatant and benzamidine-Sepharose pellet, respectively.

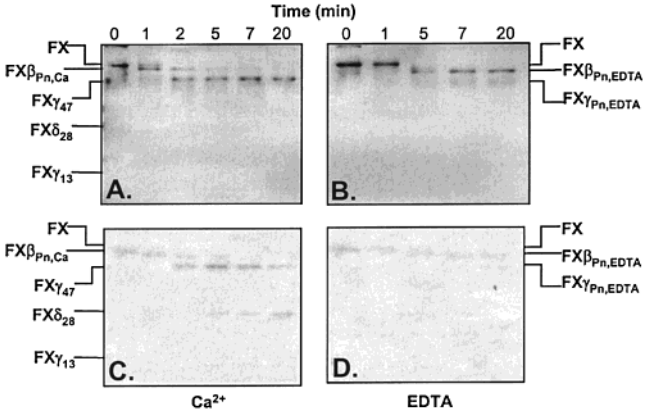

FIGURE 4: Binding of t-PA to Pn-mediated FX fragments. (A, B) Stained nonreduced SDS−PAGE (12% acrylamide); (C, D) autoradiograms. (A) FX digestion with Pn (0.1 μM) in the presence of PCPS (300 μM) and Ca^{2+} (2 mM). (B) FX digested with Pn in the presence of PCPS and EDTA (5 mM). (C) [^{125}I]t-PA (0.1 μM) binding to FX species formed in the presence of PCPS and Ca^{2+}. (D) [^{125}I]t-PA binding to FX species formed in the presence of PCPS and EDTA.

DEGR-ck into FXa$\gamma_{33/13}$ was observed by UV irradiation of the electrophoretically separated, covalently labeled products. As expected, DEGR-ck bound to the active site of plasmin-untreated FXa, labeling FXaα and FXaβ (lane 1, Figure 3A). However, DEGR-ck also bound to FXaγ_{33}, (lane 2, Figure 3A). As shown in Figure 3B, both FXaγ_{33} and FXaγ_{13} bound to benzamidine-Sepharose 6B, suggesting further that the fragments remain associated.

FX$\gamma_{47/13}$ and FXa$\gamma_{33/13}$ Binding to t-PA. Having demonstrated that FX$\gamma_{47/13}$ and FXa$\gamma_{33/13}$ remain as noncovalent heterodimers, their interaction with t-PA was examined. The rationale for these experiments was based on previous findings showing plasmin-cleaved FX and FXa accelerate t-PA activity, implying t-PA binding to plasmin-cleaved FX or FXa (*5*−*7*). To provide direct evidence for FX$\gamma_{47/13}$ or FXa$\gamma_{33/13}$ binding to t-PA, Coomassie-stained gels of FX (Figure 4, panels A and B) and FXa (Figure 5, panels A and B) cleaved in the presence of aPL and Ca^{2+} or EDTA were compared to the same [^{125}I]t-PA-probed blots. As shown in Figure 4C, t-PA bound strongly to FXγ_{47} and FXδ_{28}, and very weakly to FXγ_{13}. The major product of cleavage was FX$\gamma_{47/13}$ and we cannot account for the contributions of the

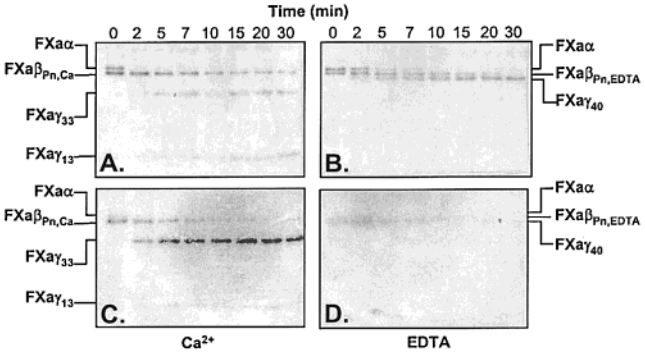

FIGURE 5: Binding of t-PA to Pn-mediated FXa fragments. (A, B) Stained nonreduced SDS−PAGE (12% acrylamide); (C, D) autoradiograms. (A) FXa digestion with Pn (0.1 μM) in the presence of PCPS (300 μM) and Ca^{2+} (2 mM). (B) FXa digested with Pn in the presence of PCPS and EDTA (5 mM). (C) [^{125}I]t-PA (0.1 μM) binding to FXa species formed in the presence of PCPS and Ca^{2+}. (D) [^{125}I]t-PA binding to FXa species formed in the presence of PCPS and EDTA

small amount of FXδ_{28} generated upon Pn treatment of FX. Binding was not observed to Pn-cleaved samples produced in the presence of EDTA (Figure 4D). As seen in Figure 5C, t-PA also bound strongly to FXaγ_{33}. FXaγ_{13} was readily detected on acrylamide gels with Coomassie staining but was only visible on blots when $\geq$ 2 μg of protein were loaded per lane, which may indicate that the fragment did not readily bind to PVDF. Nevertheless, as shown in Figure 5C, t-PA bound to FXaγ_{13}. As an indicator of specificity, when either EDTA or PC were substituted for Ca^{2+} or PCPS, respectively, the unique cleavage products did not bind [^{125}I]t-PA (results shown for EDTA cleavage). These results provided the first direct evidence that t-PA binding to Pn-cleaved FX or FXa occurs only under conditions where Ca^{2+}-dependent aPL-binding was facilitated. Thus, only the FXa and FX cleavage products predicted by N-terminal sequencing to contain C-terminal Lys residues can act as t-PA receptors.

While instructive, ligand blots are qualitative and subject to the denaturing effects of SDS−PAGE. SPR was used to demonstrate that under nondenaturing conditions, FX$\gamma_{47/13}$ and FXa$\gamma_{33/13}$ bound to immobilized t-PA (Figure 6, panels A and C). A total of 12000 RU of FXa$\gamma_{33/13}$ bound to t-PA, compared to 800 RU when the FXa was cleaved in the presence of EDTA and aPL. A total of 1500 RU of FX$\gamma_{47/13}$ bound to t-PA, compared to 800 RU when FX was cleaved in the presence of EDTA. SPR data of the interaction of aPL-depleted FX$\gamma_{47/13}$ or FXa$\gamma_{33/13}$ with t-PA did not fit any of the binding models provided by the BIAevaluation software, suggesting that t-PA immobilization may have been heterogeneous, resulting in different populations of t-PA adducts with different specificities for FX$\gamma_{47/13}$ or FXa$\gamma_{33/13}$, or alternatively a multivalent interaction between FXa$\gamma_{33/13}$ or FX$\gamma_{47/13}$ and t-PA.

FX$\gamma_{47/13}$ or FXa$\gamma_{33/13}$ Binding to Pg. FX$\gamma_{47/13}$ or FXa$\gamma_{33/13}$ which bound to t-PA were also observed by SPR to bind to Pg (Figure 6, panels B and D). FXa$\gamma_{33/13}$ bound to immobilized Pg (Figure 6B) with a total increase of 13 000 RU, compared to a total increase of 2000 RU for FXa cleaved in the presence of EDTA and aPL. Pg bound 4300 RU of FX cleaved in the presence of Ca^{2+} and aPL but 1100 RU of protein bound when the FX had been cleaved in the presence of EDTA and aPL (Figure 6D). These data demon-

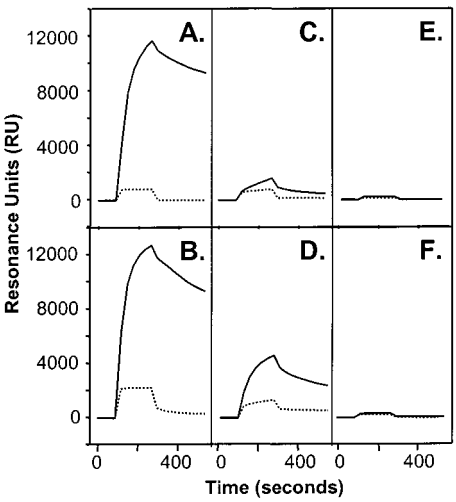

FIGURE 6: Interaction of FX$\gamma_{47/13}$ or FXa$\gamma_{33/13}$ with t-PA or plasminogen. t-PA (A, C, E) or Pg (B, D, F) were immobilized by amine coupling to carboxymethyl dextran on a BIAchip, as described in Experimental Procedures, and binding of FXa or FX cleaved by Pn in the presence of aPL (PCPS SUV) and either Ca^{2+} (solid line) or EDTA (dotted line) was followed by SPR. (A, B) FXa. (C, D) FX. (E, F) 0 FXa or FX (containing all other components of the cleavage reaction).

strated that Pn-cleaved FX and FXa fragments generated only in the presence of aPL and Ca^{2+} bound to Pg (*6*, *7*), and that SPR could be used to observe the interaction. FX$\gamma_{47/13}$ and FXa$\gamma_{33/13}$ binding to Pg was fully inhibited by co-injection with 5 mM ϵ-ACA and partially (approximately 80%) inhibited by incubation of FX$\gamma_{47/13}$ or FXa$\gamma_{33/13}$ with carboxypeptidase B (data not shown), indicating that binding was at least partially mediated by C-terminal lysine residues.

While interactions of FXa$\gamma_{33/13}$ with immobilized Pg and t-PA showed a similar extent of binding, less FX$\gamma_{47/13}$ bound to t-PA than to the Pg-coupled flow cell. This may again reflect a different affinity of FX$\gamma_{47/13}$ for t-PA or indicate that amine coupling of t-PA resulted in heterogeneous immobilization, which may have resulted in different apparent binding constants and had a greater effect on the interaction between t-PA and FX$\gamma_{47/13}$ than on FXa-derived species.

As a control for binding specificity, mixtures containing aPL, Ca^{2+} or EDTA, Pn, aprotinin, and GEMSA but no FXa or FX showed no binding to t-PA or Pg, indicating that the interaction of Pg or t-PA with FX$\gamma_{47/13}$ or FXa$\gamma_{33/13}$ was specific (Figure 6, panels E and F). To provide another control for binding, the interaction of FX$\gamma_{47/13}$ or FXa$\gamma_{33/13}$ with immobilized anti-*Salmonella* lipopolysaccharide, BSA, or uncoated dextran was tested. No binding was observed to surfaces coated with these proteins (data not shown). Species used in SPR were analyzed on SDS−PAGE and showed the expected cleavage profile (data not shown).

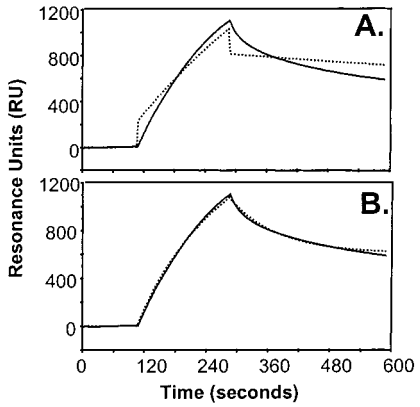

FIGURE 7: Kinetic fitting of FXa$\gamma_{33/13}$ binding to plasminogen using 1:1 and 1:2 models. SPR data was applied to a model of 1:1 binding (1 FXa$\gamma_{33/13}$:1 Pg) or 1:2 binding (1 FXa$\gamma_{33/13}$:2 Pg). (A) Sensorgram of FXa$\gamma_{33/13}$ binding to Pg (solid line), with a 1:1 fit applied (dotted line). (B) Sensorgram of FXa$\gamma_{33/13}$ binding to Pg (solid line) with a 1:2 fit applied (dotted line).

Binding Model Predicted by SPR Data Fit. SPR data describing binding and dissociation of several concentrations of FX$\gamma_{47/13}$ and FXa$\gamma_{33/13}$ to immobilized Pg was fit to first a 1:1 and then a 1:2 binding model (Experimental Procedures) (Figure 7). The kinetics of binding of FX$\gamma_{47/13}$ or FXa$\gamma_{33/13}$ to Pg best fit a model of 1:2 interaction, where one FX$\gamma_{47/13}$ or FXa$\gamma_{33/13}$ bound to 2 immobilized Pg molecules (FXa$\gamma_{33/13}$, Figure 7). This model has two association and dissociation rate constants: k_1, k_{-1}, k_2, and k_{-2} (eq 3). The final reaction showed an initial fast step followed by slower binding, as k_2 was 100-fold lower than k_1 (Table 1). The apparent dissociation constants for each experiment were calculated from the ratio of rate constants, averaged and presented in Table 1. For FXa$\gamma_{33/13}$, the apparent K_{d1} and K_{d2} were 0.4 and 30 μM for binding of the first and second Pg, respectively. For FX$\gamma_{47/13}$, the apparent K_{d1} and K_{d2} were 2.6 and 40 nM, respectively.

To determine if covalent linkage of Pg affected interaction with FXa$\gamma_{33/13}$, and provide a confirmatory estimation of K_{d1}, the amount of Pg in the presence of a constant concentration of FXa$\gamma_{33/13}$ was titrated over the flow cell surface, in competition experiments. Results showed that added solution Pg inhibited FXa$\gamma_{33/13}$ binding to immobilized Pg (Figure 8A). The amount of bound FXa$\gamma_{33/13}$ at the end of injection was plotted against free Pg included in the injection (Figure 8B). Concentration of Pg required for half-maximal inhibition of FXa$\gamma_{33/13}$ binding (I_{50}) was 0.30 ± 0.05 μM. Similarly, Pg was titrated in injections of FX$\gamma_{47/13}$ onto immobilized Pg. I_{50} for this interaction was 1.1 ± 0.3 μM. Both values are consistent with estimates of K_{d1} derived by SPR.

Calcium Dependence of FX$\gamma_{47/13}$ or FXa$\gamma_{33/13}$−Pg Interaction. Previous studies showed that cofactor activity of plasmin-cleaved aPL-bound FXa was Ca^{2+} dependent (*5*). This initial observation was refined for FX$\gamma_{47/13}$ and FXa$\gamma_{33/13}$

Table 1: Kinetics of FX$\gamma_{47/13}$ and FXa$\gamma_{33/13}$ Binding to Immobilized Pg[a]

	$k_1 \times 10^4$ (1/M s)	$k_{-1} \times 10^{-3}$ (1/s)	K_{d1} (μM)	$k_2 \times 10^2$ (1/M s)	$k_{-2} \times 10^{-4}$ (1/s)	K_{d2} (μM)
FX$\gamma_{47/13}$	0.37 ± 0.03	9.8 ± 1.6	2.6 ± 0.3	0.37 ± 0.02	0.013 ± 0.003	0.04 ± 0.006
FXa$\gamma_{33/13}$	4.8 ± 1.0	23 ± 3	0.4 ± 0.2	6.9 ± 4.7	132 ± 52	30 ± 4

[a] Results for FX$\gamma_{47/13}$ are the average ± SEM of four determinations at 120, 321, 515, or 642 nM FX$\gamma_{47/13}$, and for FXa$\gamma_{33/13}$, the average of five determinations at 25, 50, 100, 200, and 400 nM FXa$\gamma_{33/13}$.

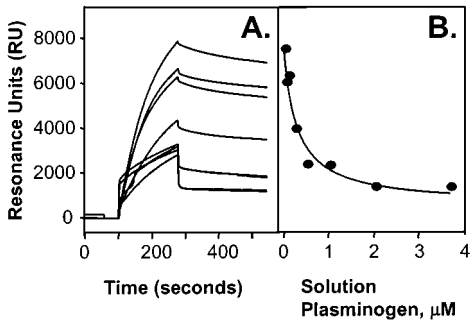

FIGURE 8: Competitive inhibition of FXa$\gamma_{33/13}$ binding to immobilized plasminogen. (A) FXa$\gamma_{33/13}$ prepared on SUV as described in Experimental Procedures, was diluted to 0.625 μM in SPR running buffer containing 2 mM Ca^{2+} and combined with 0, 0.05, 0.25, 0.5, 1, 2, or 3.7 μM of Pg, corresponding to the points shown in panel B. (B) Resonance units (RU) at the start of dissociation (5 s after the end of injection) represented amount of bound protein and were correlated to amount of Pg added, to determine I_{50}.

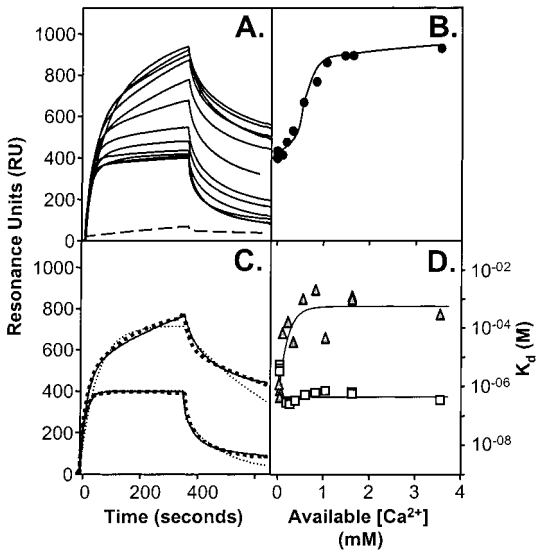

FIGURE 9: Calcium-dependence of FXa$\gamma_{33/13}$−Pg interaction. (A) FXa$\gamma_{33/13}$ (0.2 μM) was injected over 2000 RU of immobilized Pg (solid lines) in 0, 0.1, 0.5, 0.6, 0.75, 1.0, 1.2, 1.4, 2, and 4 mM Ca^{2+}. FXa$\gamma_{33/13}$ was also injected in 2 mM Ca^{2+} over uncoated dextran (dotted line). (B) RU at 6 min was plotted vs available Ca^{2+} to show that half-maximal Ca^{2+} dependence of the FXa$\gamma_{33/13}$−Pg interaction was approximately 0.6 mM. (●) Pg surface. (C) SPR data at 1.4 and 0 mM Ca^{2+} (solid black line), 1:1 fit (thin dotted line) and 1:2 fit (thick dotted line). (D) Apparent dissociation constants obtained from 1:2 fit of SPR data at different concentrations of Ca^{2+}. Open squares, K_{d1}; gray triangles, K_{d2}.

using SPR. aPL-depleted FX$\gamma_{47/13}$ and FXa$\gamma_{33/13}$ were equilibrated at various concentrations of Ca^{2+} and injected over immobilized Pg at the same concentration of Ca^{2+} used for equilibration. Data were plotted to reflect the changes in binding observed at different Ca^{2+} concentrations, corrected for residual EDTA in FX$\gamma_{47/13}$ and FXa$\gamma_{33/13}$ samples. At 0 Ca^{2+} and in the presence of 5 mM EDTA, FX$\gamma_{47/13}$ and FXa$\gamma_{33/13}$ bound to Pg, indicating Ca^{2+}-independent interactions. Binding was enhanced by Ca^{2+}, with half-maximal effect at approximately 0.6 mM, for both FXa$\gamma_{33/13}$ (Figure 9) and FX$\gamma_{47/13}$ (not shown).

Since at 2 mM Ca^{2+}, SPR data fit a model of 1:2 binding, we hypothesized that lower binding at reduced calcium concentrations was due to a change in FXa resulting in removal of one binding site. To test this hypothesis, we fit the data summarized in Figure 9A (Ca^{2+} titration) to both 1:1 and 1:2 models. Data fit the 1:1 model more closely at low [Ca^{2+}] but was still better described by the 1:2 model at all concentrations of Ca^{2+} (Figure 9C). As Ca^{2+} increased, K_{d1} and K_{d2} derived from fitting all data to the 1:2 model decreased and increased, respectively (Figure 9D). Both effects showed saturation at high concentrations of Ca^{2+}, with half-maximal effect occurring at or below 0.2 mM Ca^{2+}.

DISCUSSION

Earlier work from our laboratory showed several effects of Pn on FX and FXa, including inhibition of coagulation function, acquisition of t-PA cofactor activity and differential cleavage when bound to aPL (*5*−*7*). To further understand the molecular basis of the functional transition conferred by Pn to FX and FXa, the goals of the current project were (a) to determine if the Pn-mediated fragments of aPL-bound FX or FXa remain noncovalently associated, (b) to determine whether they directly bound t-PA, and (c) to quantify their interaction with Pg.

FX$\gamma_{47/13}$ and FXa$\gamma_{33/13}$ were initially characterized on the basis of Ca^{2+}-dependent aPL affinity of their Gla-domain, located on FXγ_{47} or FXaγ_{33}. Affinity fractionation using PCPS LV showed that FXγ_{13} or FXaγ_{13} co-localized with FXγ_{47} or FXaγ_{33}, respectively, implying they were noncovalent heterodimers. Further structural characterization used the active site probes DEGR-ck and benzamidine. DEGR-ck binding requires the entire FXa active site (*28*). Since FXa$\gamma_{33/13}$ contains His^{236} and Asp^{282} in FXaγ_{33} and Ser^{379} in FXaγ_{13} (*6*), covalent incorporation of DEGR-ck into FXaγ_{33} demonstrated that FXaγ_{33} and FXaγ_{13} remained associated, implying that the region of FXa$\gamma_{33/13}$ corresponding to the active site of FXa retained structural integrity. The benzamidine binding site [i.e., P1 specificity pocket (*29*,*30*)] is contained almost exclusively in FXaγ_{13}. Intact FXa$\gamma_{33/13}$ bound to benzamidine-Sepharose, further showing that FXa$\gamma_{33/13}$ was a noncovalent heterodimer. These results agree with a previous report of DEGR-ck and *para*-aminobenzamidine (*p*-AB) binding to a 1:1 mixture of FXaβ and FXa autolytically cleaved at Arg^{332}; however, the noncovalent subunit association of cleaved FXa was not investigated (*11*).

To explain the basis of maintaining an interaction between FXaγ_{33} and FXaγ_{13}, the FXa structure reported by Padmanabhan et al. (*28*) provides a useful model of FXa$\gamma_{33/13}$. The protein was cleaved in the autolysis loop and lacked resolvable structure between His^{327} and Ser^{334}. His^{327} is only two residues away from the predicted site of Pn cleavage (Lys^{330}) (*6*). This structure was analyzed to explore the hydrogen bond interactions between FXaγ_{33} and FXaγ_{13} (Figure 10, panels A and B). The structure showed a network of 34 hydrogen bonds between FXaγ_{33} and FXaγ_{13}. Interestingly, 22 of these were localized to the C-terminus of FXaγ_{33} and the N-terminus of FXaγ_{13}, thereby stabilizing the effects of Lys^{330} peptide bond cleavage by Pn.

While structural characterization showed that FXa$\gamma_{33/13}$ is a noncovalent heterodimer, it did not explain why FXa$\gamma_{33/13}$ shows reduced hydrolysis of tripeptidyl chromogenic substrate (*5*, *7*, *11*). To determine whether reduced catalytic activity of FXa$\gamma_{33/13}$ could be correlated to active site changes, published structures of FXa obtained from different

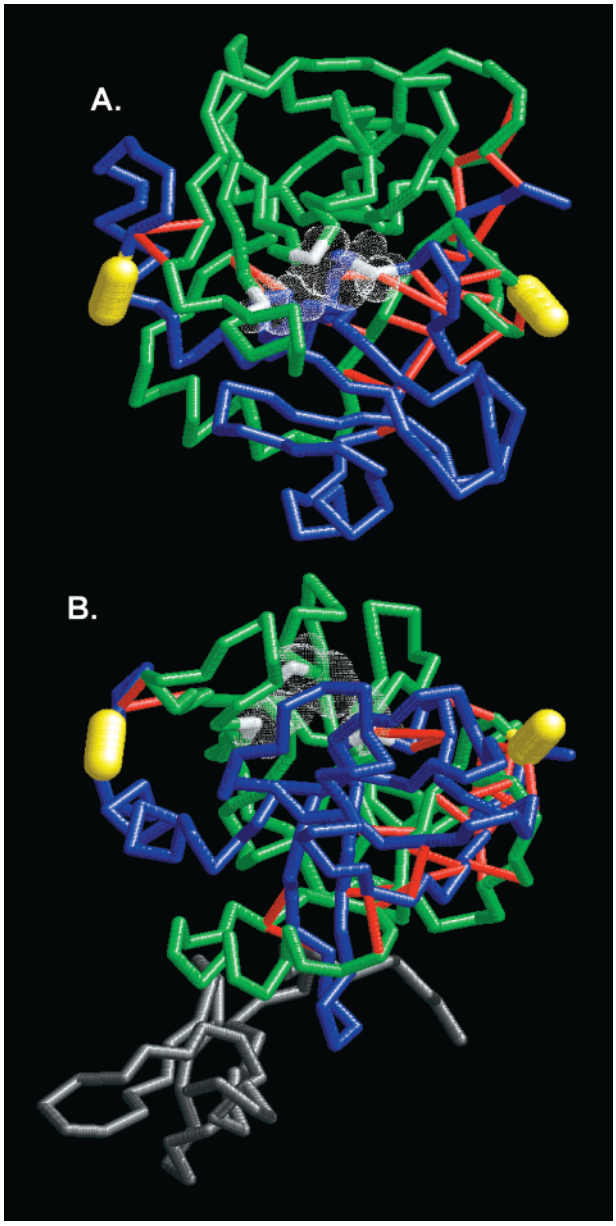

FIGURE 10: Hydrogen bonds stabilize the FXa$\gamma_{33/13}$ heterodimer. C-Terminal lysines are located on opposite sides of the molecule. Based on the X-ray crystallographic structure obtained by (*28*). FXaγ_{33}, green chain. FXaγ_{13}, blue chain. C-Terminal lysine residues are shown at their predicted locations, highlighted in yellow. Hydrogen bonds stabilizing interactions between FXaγ_{33} and FXaγ_{13} are shown in red. Ser^{379}, Arg^{282}, and His^{236} at the active site are dotted in white. (A) Top view of FXa$\gamma_{33/13}$, in the plane of the membrane. The light chain is not shown for clarity. (B) side view of FXa$\gamma_{33/13}$, perpendicular to the plane of the membrane. The top of the light chain, which contains the aPL-binding domain, is depicted in gray. C-terminal lysine residues produced by Pn cleavage are on opposite sides of the FXa molecule and point away from the membrane. Depicted using Rasmol 2.

sources were compared. Autolysis loop-cleaved human FXa, derived by Padmanabhan et al. (*28*) provided a model for FXa$\gamma_{33/13}$. This was compared to uncleaved active-site inhibited FXa (*31*). The aligned active sites (not shown) were nearly identical, with only minor differences in the position of the active site Ser^{379} hydroxyl residue, potentially only reflecting the normal flexibility of this bond. The changes to the FXa active site after Pn cleavage responsible for lost chromogenic activity are accordingly subtle. Studies showing binding of *p*-AB to FXa cleaved at Arg^{332} reported a significantly quenched fluorescence spectrum compared to intact FXa, implying structural differences between cleaved and intact FXa, despite only slightly altered *p*-AB binding affinity (*11*).

An essential component of Pg cofactors is the presence of a C-terminal lysine residue (*5*, *12*−*20*) to which Pg binds primarily by its kringle-1 and kringle-4 domains (*32*). t-PA possesses two kringle domains, the second of which also mediates binding to C-terminal lysines (*33*). Since both subunits of FX$\gamma_{47/13}$ and FXa$\gamma_{33/13}$ have C-terminal lysine residues, it was hypothesized that t-PA could bind to FX$\gamma_{47/13}$ or FXa$\gamma_{33/13}$. This interaction was shown for the first time, using both ligand blot and SPR studies.

Consistent with earlier ligand blot data (*6*), observations with Pg showed specific interaction between FX$\gamma_{47/13}$ or FXa$\gamma_{33/13}$ and Pg, reflecting the differential cleavage of FX or FXa by Pn when bound to aPL, compared to not bound. Using SPR, the interaction of well-characterized FX$\gamma_{47/13}$ or FXa$\gamma_{33/13}$ with Pg was quantified for the first time. Experiments using various concentrations of aPL-depleted FX$\gamma_{47/13}$ of FXa$\gamma_{33/13}$ to follow Pg binding fit well to a model where two Pg molecules bound per molecule of FX$\gamma_{47/13}$ or FXa$\gamma_{33/13}$. The fit for FXa$\gamma_{33/13}$ predicts rapid formation of a 1:1 complex of FXa$\gamma_{33/13}$:Pg ($K_{d1} = 0.4\ \mu M$), followed by slower, weaker binding of a second Pg (1 FXa$\gamma_{33/13}$:2 Pg) ($K_{d2} = 30\ \mu M$). By contrast, at almost 5-fold higher, the K_{d1} for FX$\gamma_{47/13}$ reflects the lower rate of binding observed in qualitative evaluations using SPR (Figure 6). Formation of a 1:2 complex of FX$\gamma_{47/13}$:$(Pg)_2$ was estimated to be tighter, with $K_{d2} = 40$ nM. The rate-limiting step for both FX$\gamma_{47/13}$ and FXa$\gamma_{33/13}$ association with Pg was formation of the trimolecular complex, while the rate of dissociation of the complex was calculated to be much lower for FX$\gamma_{47/13}$-$(Pg)_2$ than for FXa$\gamma_{33/13}$-$(Pg)_2$. The difference in apparent K_{d1} between FX$\gamma_{47/13}$ and FXa$\gamma_{33/13}$ for Pg may be due to steric hindrance of Pg binding to FX$\gamma_{47/13}$ by the activation peptide. Recently, the activation peptide was suggested to block a putative FVa binding site (the region surrounding Asp_{348}), accounting for the lower binding of FVa by FX, compared to FXa (*34*). The location of this suggested FVa binding site (residues 346−349), between Lys_{330} and Lys_{435}, may implicate the activation peptide in reducing FX$\gamma_{47/13}$ binding to Pg. However, studies using synthetic peptides corresponding to residues 263−276 (*35*) and 253−277 and FXa cleaved at Arg^{332} (*11*) have implicated additional FXa regions in this interaction.

In another measure of the interaction between Pg and FX$\gamma_{47/13}$ or FXa$\gamma_{33/13}$, solution-phase Pg was added to inhibit FX$\gamma_{47/13}$ or FXa$\gamma_{33/13}$ binding to immobilized Pg. The derived I_{50} values for Pg were comparable to K_{d1} values derived from the SPR kinetics (Table 1) for both FX$\gamma_{47/13}$ and FXa$\gamma_{33/13}$. The agreement between these values, together with the derived K_d in separate experiments for [^{125}I]Pg binding to Pn-cleaved FXa on aPL-coated microtiter plate wells (0.29 μM) (*5*) suggests that immobilized Pg was not denatured or bound heterogeneously to the BIAchip flow cell in SPR experiments. Since this assay was performed in the presence of aPL, these data indicate that avidity effects were not present at the concentration of PCPS used in this assay, which was 38 μM. In contrast, when 1 μM of PCPS was used to increase the number of molecules of FXa$\gamma_{33/13}$ per vesicle,

the interaction of FXa$\gamma_{33/13}$ with immobilized Pg had an apparent K_d of 4.4 nM (not shown), suggesting possible avidity effects may significantly enhance the apparent physiological affinities due to local concentration effects. The apparent K_d for the interaction of Pg with FXa fragments was comparable to the K_d for the interaction of Pg with fibrin [0.32 μM (*36*)], endothelial Pg receptor [0.11 μM (*37*)] fibronectin [0.09 μM (*38*)] and bone osteonectin [0.12 μM (*19*)], suggesting similar types of binding mediate these interactions.

The interaction of FX$\gamma_{47/13}$ and FXa$\gamma_{33/13}$ with Pg and t-PA was shown to be mediated partly by C-terminal lysine residues, in agreement with the results of ligand blotting, sequencing, and chromogenic functional assays, which predicted their involvement (*5*−*7*). The two C-terminal lysine residues in FXa$\gamma_{33/13}$ are localized by molecular modeling at opposite ends of the catalytic domain, each optimally accessible for Pg binding (Figure 10A) and distal from the predicted spatial orientation relative to the membrane (Figure 10B). This configuration supports the mathematical model suggesting binding of two Pg to each molecule of FX$\gamma_{47/13}$ or FXa$\gamma_{33/13}$, which is in agreement with [^{125}I]Pg blots revealing binding to both subunits (*6*, *7*; unpublished data). Since we show that [^{125}I]t-PA can bind both fragments within FX$\gamma_{47/13}$ or FX$\gamma_{33/13}$, this may indicate a similar 2:1 model could be applied to the t-PA interactions. An additional possibility is formation of a 1:1:1 ternary complex between Pg, t-PA and Pn-cleaved FX or FXa.

A surprising finding from our experiments was that Ca^{2+} enhanced binding of FX$\gamma_{47/13}$ or FXa$\gamma_{33/13}$ to Pg by nearly 2-fold (Figure 9). To our knowledge, no other t-PA cofactor shows Ca^{2+}-enhancement. Even annexin II tetramer, which, like FXa, shows all other in vitro activities to be Ca^{2+}-dependent, stimulates t-PA in a Ca^{2+}-independent manner (*39*). FXa undergoes a well-known Ca^{2+}-mediated structural transition (*40*), and FX$\gamma_{47/13}$ or FXa$\gamma_{33/13}$ may also undergo the same or similar changes, which in turn may enhance Pg binding. The binding observed at low Ca^{2+} concentrations cannot be kinetically described simply as 1:1, indicating the interaction is likely governed by more complex interactions. The results of this analysis support our suggestion that FX$\gamma_{47/13}$ or FXa$\gamma_{33/13}$ may undergo Ca^{2+}-dependent changes similar to the uncleaved protein. In agreement, the intrinsic association of FXa and FVa is enhanced by Ca^{2+} (*24*), which is believed to involve the region in FXa cleaved by Pn (*11*). The protease domain of FXa has a high affinity Ca^{2+} binding site predicted to lie within residues 249−260 (*11*). The overlap of this site with the aforementioned putative FVa binding site may be relevant to the loss of activity after autolysis loop cleavage. A possible significance of the effect of Ca^{2+} on FX$\gamma_{47/13}$ and FXa$\gamma_{33/13}$ binding to Pg is that it would further localize binding to areas of high local Ca^{2+}, such as at the site of clot, and to membrane-bound FXa$\gamma_{33/13}$.

Since Pn-mediated cofactor activity is only produced in the presence of aPL and Ca^{2+}, in a physiological setting, generation of FX$\gamma_{47/13}$ and FXa$\gamma_{33/13}$ would occur only at the site of clot. The intact Gla domain of FX$\gamma_{47/13}$ or FXa$\gamma_{33/13}$ would localize the site of catalytic complex to aPL. Since the primary cofactor for t-PA acceleration is predicted to be plasmin-cleaved fibrin, the relevance of FX$\gamma_{47/13}$ or FXa$\gamma_{33/13}$ to clot dissolution may be to provide the first few C-terminal lysine residues for initial rapid generation of plasmin to overcome an antifibrinolytic threshold. This role has been suggested for autolytically produced FXaβ in a "tick-over" mechanism (*6*) to facilitate sequential Pg binding, Pn production, anticoagulation of FX and FXa and production of FX$\gamma_{47/13}$ and FXa$\gamma_{33/13}$. A preponderance of evidence exists to show localization of Pg receptors to cell surfaces such as circulating blood cells, endothelial cells, fibroblasts and hepatocytes (*41*) or extracellular matrix (e.g., refs *14*−*16*, *19*, *20*, *37*, *41*−*43*). The major difference between these receptors and FX$\gamma_{47/13}$ and FXa$\gamma_{33/13}$ is that Pn creates a t-PA accelerator by modulating key coagulation factors, localizing Pn production to the site of thrombin production and simultaneously functioning as an anticoagulant. We propose that this feedback mechanism would contribute to ensure the sequential activation of coagulation and then fibrinolysis.

ACKNOWLEDGMENT

We gratefully acknowledge Dr. Maria Issa (Canadian Blood Services, Vancouver, British Columbia) for size determination of sucrose-loaded PCPS vesicles, Allan Menzies and Larry Whitehouse (Health Canada, Ottawa, Ontario) for their assistance and use of the BIAcore 3000, and Christina Raynor for critical reading of the manuscript.

REFERENCES

1. Messier, T. L., Pittman, D. D., Long, G. L., Kaufman, R. J., and Church, W. R. (1991) *Gene 99*, 291.
2. Leytus, S. P., Kurachi, K., Sakariassen, K. S., and Davie, E. W. (1986) *Biochemistry 25* (17), 4855.
3. Lindhout, M. J., and Hemker, H. C. (1978) *Biochim. Biophys Acta 533*, 318.
4. Skogen, W. F., Esmon, C. T., and Cox, A. C. (1984) *J. Biol. Chem. 259*, 2306.
5. Pryzdial, E. L. G., Bajzar, L., and Nesheim, M. E. (1995) *J. Biol. Chem. 270*, 17871.
6. Pryzdial, E. L. G., and Kessler, G. E. (1996) *J. Biol. Chem. 271*, 16614.
7. Pryzdial, E. L. G., Lavigne, N., Dupuis, N., and Kessler, G. (1999) *J. Biol. Chem. 274*, 8500.
8. Jesty, J., Spencer, A. K., and Nemerson, Y. (1974) *J. Biol. Chem. 249*, 5614.
9. Fujikawa, K., Coan, M. H., Legaz, M. E., and Davie, E. W. (1974) *Biochemistry 13*, 5290.
10. Fujikawa, K., Titani, K., and Davie, E. W. (1975) *Proc. Natl. Acad. Sci. U.S.A. 72*, 3359.
11. Sabharwal, A. K., Padmanabhan, K., Tulinsky, A., Mathur, A., Gorka, J., and Bajaj, S. P. (1997) *J. Biol. Chem. 272*, 22037.
12. Plow, E. F., Felez, J., and Miles, L. A. (1991) *Thromb. Haemost. 66*, 32.
13. Hajjar, K. A., and Nachman, R. L. (1994) in *Hemostasis and thrombosis. Basic principles and clinical practice* (Colman, R. W., Hirsh, J., Marder, V. J., and Salzman, E. W., Eds.) pp 823−836, J. B. Lippincott Company, Philadelphia.
14. Miles, L. A., Dahlberg, C. M., Plescia, J., Felez, J., Kato, K., and Plow, E. F. (1991) *Biochemistry 30*, 1682.
15. Hajjar, K. A., Jacovina, A. T., and Chacko, J. (1994) *J. Biol. Chem. 269*, 21191.
16. Cesarman, G. M., Guevara, C. A., and Hajjar, K. A. (1994) *J. Biol. Chem. 269*, 21198.
17. Dudani, A. K., Cummings, C., Hashemi, S., and Ganz, P. R. (1993) *Thromb. Res. 69*, 185.
18. Dudani, A. K., Pluskota, A., and Ganz, P. R. (1994) *Biochem. Cell. Biol. 72*, 126.
19. Kelm, R. J., Jr., Swords, N. A., Orfeo, T., and Mann, K. G. (1994) *J. Biol. Chem. 269*, 30147.
20. Reinartz, J., Hansch, G. M., and Kramer, M. D. (1995) *J. Immunol. 154*, 844.

21. Higgins, D. L., and Mann, K. G. (1983) *J Biol Chem. 258*, 6503.
22. Gomori, G. (1942) *J. Lab. Clin. Med. 27*, 955.
23. Krishnaswamy, S., Jones, K. C., and Mann, K. G. (1988) *J. Biol. Chem. 263*, 3823.
24. Pryzdial, E. L. G., and Mann, K. G. (1991) *J. Biol. Chem. 266*, 8969.
25. Jönsson, U., Fägerstam, L., Ivarsson, B., Johnsson, B., Karlsson, R., Lundh, K., Löfås, S., Persson, B., Roos, H., Rönnberg, I., Sjölander, S., Stenberg, E., Ståhlberg, R., Urbaniczky, C., Östlin, H., and Malmqvist, M. (1991) *Biotechniques 11* (5), 620.
26. Mackenzie, C. R., Hirama, T., Lee, K. K., Altman, E., and Young, N. M. (1997) *J. Biol. Chem. 272* (9), 5533.
27. Cooper, M. A., and Williams, D. H. (1999) *Anal. Biochem. 276*, 36.
28. Padmanabhan, K., Padmanabhan, K. P., Tulinsky, A., Park, C. H., Bode, W., Huber, R., Blankenship, D. T., Cardin, A. D., and Kisiel, W. (1993) *J. Mol. Biol. 232*, 947.
29. Geratz, J. D., Stevens, F. M., Polakoski, K. L., Parrish, R. F., and Tidwell, R. R. (1979) *Arch. Biochem. Biophys. 197* (2), 551.
30. Monroe, D. M., Sherrill, G. B., and Roberts, H. R. (1988) *Anal. Biochem. 172*, 427.
31. Brandstetter, H., Kühne, A., Bode, W., Huber, R., von der Saal, W., Wirthensohn, K., and Engh, R. A. (1996) *J. Biol. Chem. 271* (47), 29988.
32. de Munk, G. A., Caspers, M. P., Chang, G. T., Pouwels, P. H., Enger-Valk, B. E., and Verheijen, J. H. (1989) *Biochemistry 28* (18), 7318.
33. van Zonneveld, A. J., Veerman, H., and Pannekoek, H. (1986) *J. Biol. Chem. 261* (30), 14214.
34. Rudolph, A. E., Porche-Sorbet, R. M., and Miletich, J. P. (2000) *Biochemistry 39*, 2861.
35. Chattopadhyay, A., James, H. L., and Fair, D. S. (1992) *J. Biol. Chem. 267*, 12323.
36. Harpel, P. C., Chang, T.-S., and Verderber, E. (1985) *J. Biol. Chem. 260* (7), 4432.
37. Dudani, A. K., Cummings, C., Hashemi, S., and Ganz, P. R. (1993) *Thromb. Res 69*, 185.
38. Salonen, E.-M., Saksela, O., Vartio, T., Vaheri, A., Nielsen, L. S., and Zeuthen, J. (1985) *J. Biol. Chem. 260* (22), 12302.
39. Kassam, G., Choi, K.-S., Ghuman, J., Kang, H.-M., Fitzpatrick, S. L., Zackson, T., Zackson, S., Toba, M., Shinomiya, A., and Waisman, D. M. (1998) *J. Biol. Chem. 273*, 4790.
40. Radcliffe, R. D., and Barton, P. (1973) *J. Biol. Chem. 248*, 6788.
41. Felez, J. (1998) *Fibrinol. Proteol. 12* (4), 183.
42. Kost, C., Benner, K., Stockmann, A., Linder, D., and Preissner, K. (1996) *Eur. J. Biochem. 236*, 682.
43. Gonzalez-Gronow, M., Stack, S., and Pizzo, S. V. (1991) *Arch. Biochem. Biophys. 286*, 625.

BI002209V